Available online at www.sciencedirect.com
SCIENCE DIRECT®
International Journal of Thermal Sciences 45 (2006) 782–795
International Journal of Thermal Sciences
www.elsevier.com/locate/ijts

Flow mode-transition of natural convection in inclined rectangular enclosures subjected to bidirectional temperature gradients

H. Wang, M.S. Hamed *

Thermal Processing Laboratory, Department of Mechanical Engineering, McMaster University, Hamilton, ON, L8S 4L7, Canada

Received 10 August 2004; received in revised form 1 July 2005; accepted 11 July 2005

Available online 19 December 2005

Abstract

Steady two-dimensional natural convection in air-filled, rectangular, inclined enclosures has been investigated numerically. Conservation of mass, momentum, and energy equations have been solved using finite volume approach employing a staggered grid arrangement. The physical covariant velocity components and temperature have been selected as the independent variables in the momentum and energy equations and the coupling between the continuity and momentum equations has been accounted for using the SIMPLE algorithm.

The effect of various configurations of bidirectional temperature gradients on mode transition of thermal convection inside the cavity has been investigated. Numerical treatment of temperature discontinuity at the corner points of the cavity and its effect on the calculated Nusselt number has been discussed.

Simulations have been carried out for Rayleigh numbers in the range between 10^3 and 10^4, aspect ratio (width/height) $= 4$, and angle of inclination between 0 and 90°. Results indicate that thermal conditions of cavity end walls have a significant effect on mode-transition of thermal convection flows; and hence, on heat transfer effectiveness inside the cavity, and on the Hysteresis phenomenon (multi-steady solutions) occurred as the cavity angle of inclination (γ) varied. The existence of such multi-steady solutions strongly depends on the value of Rayleigh number.

Keywords: Natural convection; Inclined rectangular enclosures; Bidirectional temperature gradients; Flow mode-transition

1. Introduction

Natural convection in closed enclosures has been extensively studied numerically and experimentally [1–4]. The study of thermal convection in inclined enclosures is motivated by a desire to find out what effect slope would have on certain thermally driven flows which are found in many engineering applications. These applications include: building systems containing multi-layered walls, double windows, and air gaps in unventilated spaces; energy systems such as solar collectors, storage devices, furnaces, heat exchangers, and nuclear reactors; material processing equipment such as melting and crystal growth reactors. Thermally driven flows are also found in large scale geophysical, astrophysical, and environmental phenomena.

Most of the research work that has been carried out in this area was focused on enclosures that were differentially heated in one direction (vertically or horizontally) with adiabatic side walls in the other direction. Rather little work has been carried out considering more complex thermal boundary conditions that are normally found in most of the aforementioned practical applications. In these applications, the imposed temperature gradient is neither horizontal nor vertical. Ostrach [4], in his review on natural convection in enclosures, noted that configurations with more complex boundary conditions can be viewed as an exception among the works on this topic.

Thermal convection in enclosures heated from below and cooled from above is of special interest because of flow mode-transition that had been observed and reported by many researchers [5,6]. Corcione [7] carried out a numerical investigation on the effect of various thermal conditions of cavity side walls on flow-mode transition of natural convection in rectangular horizontal enclosures, heated from below and cooled on the top. Different width-height aspect ratios were considered.

* Corresponding author. Tel.: +1 905 525 9140 ext. 26113; fax: +1 905 572 7944.

E-mail address: hamedm@mcmaster.ca (M.S. Hamed).

1290-0729/$ – see front matter
doi:10.1016/j.ijthermalsci.2005.07.008

Nomenclature

A	aspect ratio, $= LH^{-1}$
g	gravitational acceleration
H	cavity height
L	cavity length
Nu	Nusselt number
P	pressure
p	dimensionless pressure, $= P(\rho U^{*2})^{-1}$
Pr	Prandtl number
Q_{in}	sum of heat transferred from hot wall(s)
Q_{out}	sum of heat transferred to cold wall(s)
Ra	Rayleigh number, $= g\beta(T_h - T_c)H^3\alpha^{-1}\nu^{-1}$
U^*	characteristic velocity (velocity scale), $= \nu H^{-1}$
u	component of dimensionless velocity in x-direction, $= UU^{*-1}$
v	component of dimensionless velocity in y-direc tion, $= VU^{*-1}$
X, Y	Cartesian coordinates
x, y	dimensionless coordinates, $= XH^{-1}$, and YH^{-1}, respectively

Greek symbols

α	thermal diffusivity
β	coefficient of thermal expansion, $= -(\partial\rho/\partial T)_P\rho^{-1}$
γ	angle of inclination of cavity (measured from horizontal line)
ψ	stream function
θ	dimensionless temperature, $= (T - T_c)(T_h - T_c)^{-1}$
ρ	density
ν	kinematic viscosity

Subscript

ave	average value
c	cold surface
h	hot surface
max	maximum value
min	minimum value
x	component in x-direction
y	component in y-direction

Rayleigh numbers, based on cavity height, were between 10^3 to 10^6. Corcione's results have shown that bidirectional differential heating has a significant effect on flow mode-transition of natural convection inside horizontal cavities. Some of these bidirectional differential heating configurations considered in [7] involved temperature discontinuities at the cavity corners. No discussion was provided on the effect of these temperature discontinuities on the calculated Nusselt numbers.

Soong and Tzeng [8] numerically investigated the effect of angle of inclination on flow mode-transition in an inclined rectangular enclosure heated from below and cooled from above with two insulated side walls. Different aspect ratios were considered and Rayleigh number ranged from 1.5×10^3 to 2×10^4. Flow mode-transition and Hysteresis phenomenon for $Ra >$ 2000 have been demonstrated.

In real life applications, end walls are never perfectly insulated. In light of results reported in [7,8], there might be conditions by which heat transfer effectiveness inside the cavity could be altered in a desired way by using different configurations of bidirectional temperature gradients (i.e., by changing thermal conditions of cavity end walls) combined with changing cavity angle of inclination. Hence, the main objective of this study is to investigate the combined effect of various bidirectional temperature gradients and angles of inclination on flow mode-transition and on hysteresis phenomenon (multi-steady solutions) in rectangular enclosures. Such combined effect, to the authors' knowledge, has not been investigated yet.

2. Problem formulation

Consider a rectangular cavity of length L and height H as shown in Fig. 1. The cavity is filled with air and its bottom and top walls are maintained at T_h and T_c, respectively. End walls are maintained at different thermal boundary conditions

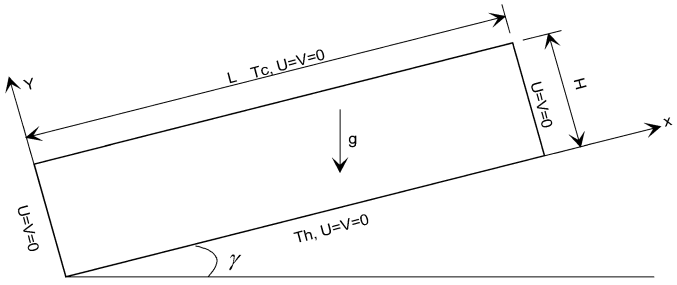

Fig. 1. The model problem.

depending on the configuration of bidirectional temperature gradient considered. In addition to the base case of insulated end walls, denoted here as AA configuration, three configurations of end wall thermal conditions have been considered in the present study. As shown in Fig. 2, these three configurations are denoted by CH, CC, and HH. In the CC and HH configurations, both end walls are maintained at constant temperatures of T_c or T_h, respectively. The left and right end walls are maintained at T_c and T_h in the CH configuration.

Steady, two-dimensional natural convection flow inside the cavity, assuming constant properties and employing the Boussinesq approximation for the gravity term, is governed by the following set of dimensionless equations:

$$\frac{\partial u}{\partial x} + \frac{\partial v}{\partial y} = 0 \tag{1}$$

$$u\frac{\partial u}{\partial x} + v\frac{\partial u}{\partial y} = -\frac{\partial p}{\partial x} + \frac{\partial^2 u}{\partial x^2} + \frac{\partial^2 u}{\partial y^2} + Ra \times \frac{1}{Pr} \times \theta \times \operatorname{Sin}\gamma \tag{2}$$

$$u\frac{\partial v}{\partial x} + v\frac{\partial v}{\partial y} = -\frac{\partial p}{\partial y} + \frac{\partial^2 v}{\partial x^2} + \frac{\partial^2 v}{\partial y^2} + Ra \times \frac{1}{Pr} \times \theta \times \operatorname{Cos}\gamma \tag{3}$$

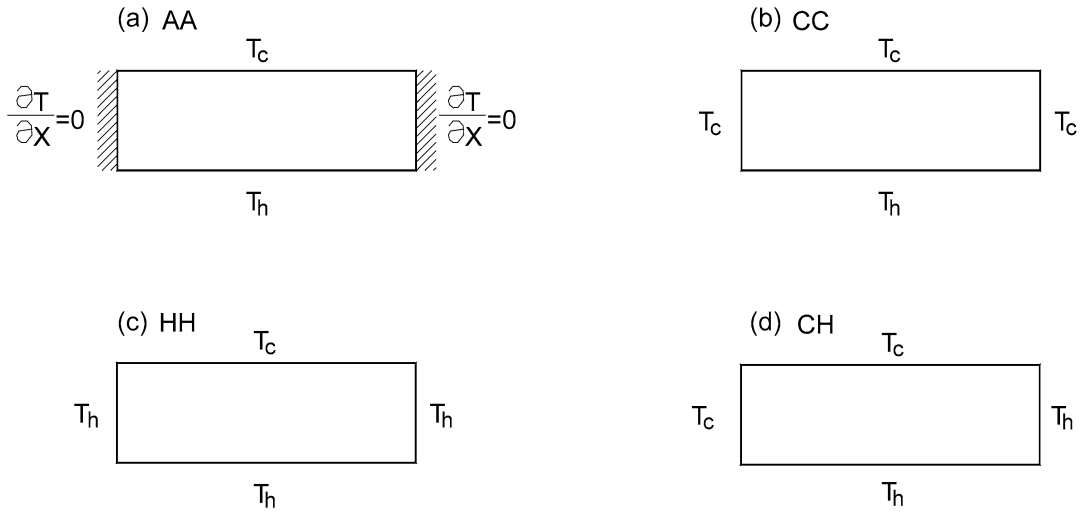

Fig. 2. The four configurations of bidirectional temperature gradients considered in the present study.

$$u\frac{\partial\theta}{\partial x}+v\frac{\partial\theta}{\partial y}=\frac{1}{Pr}\left(\frac{\partial^2\theta}{\partial x^2}+\frac{\partial^2\theta}{\partial y^2}\right) \tag{4}$$

Eq. (1) is the continuity equation. Eqs. (2)–(4) are the x-momentum, y-momentum, and the energy equation, respectively. Velocity boundary conditions for Eqs. (1)–(4) are shown in Fig. 1.

Nusselt number was calculated using the following equations:

x-direction:

$$Nu_x=\frac{1}{A}\int_o^A\left.\frac{\partial\theta}{\partial y}\right|_{\text{wall}}\mathrm{d}x \tag{5}$$

y-direction:

$$Nu_y=\int_0^1\left.\frac{\partial\theta}{\partial x}\right|_{\text{wall}}\mathrm{d}y \tag{6}$$

3. Numerical algorithm

Eqs. (1)–(4) subject to boundary conditions shown in Figs. 1 and 2 were solved by using finite volume method and the SIMPLE algorithm [9]. The procedure was regarded converged when maximum difference of all independent variables (u, v, p, and θ) and maximum change in calculated average Nusselt number between two successive iterations were less than 10^{-5}. The error in the energy balance of the whole cavity was calculated from:

$$Q_{\text{error}}=\left|\frac{|Q_{\text{out}}|-|Q_{\text{in}}|}{\text{Min}(|Q_{\text{out}}|,|Q_{\text{in}}|)}\right| \tag{7}$$

and $Q_{\text{error}}<1\%$ was an additional condition required to consider the procedure convergent.

4. Domain discretization

The computational domain in each of the x- and y-directions was subdivided into three subsections, two narrow sections

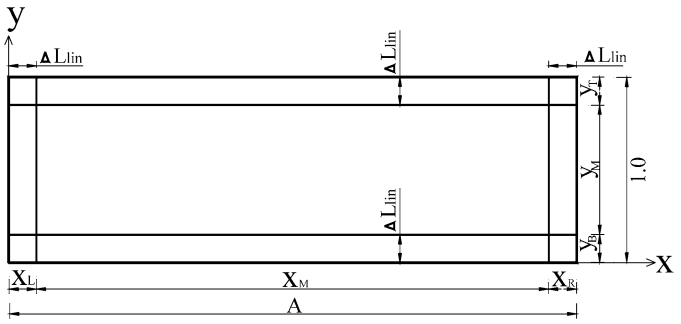

Fig. 3. Arrangement of grid points in the computational domain.

along the side walls, the width of each of which equals to ΔL_{lin}, and a relatively wide section in the middle of the cavity, as depicted in Fig. 3. A uniform, staggered grid according to practice A in [9] was adopted in all subsections. Grids were distributed according to the following scheme: 10% of the total number of grid points used in each direction was uniformly distributed in each of the two near-wall subsections (X_L and X_R and Y_T and Y_B, in the x- and y-directions, respectively). The remainder of the grid points (i.e., 80%) was uniformly distributed in the middle subsections, X_m and Y_M. The effect of using various values of ΔL_{lin} was investigated as part of the procedure of treating temperature discontinuities at cavity corners which will be discussed in the next section.

5. Treatment of temperature discontinuity at corner points

Although temperature discontinuities at corner points has found to have no influence on the numerical calculations of the flow field and the internal temperature field (see values of $u_{\max}$, $v_{\max}$, and $\psi_{\max}$ in Table 1), it had a significant effect on the calculation of Nusselt number. As reported in [10], due to temperature discontinuities, the calculated heat flux exhibits a non-integrable singularity at corner points and consequently the overall rate of heat transfer turns out to be unbounded. Accordingly, Nusselt number becomes larger and larger as the grid is refined. Some authors, e.g., [7], adopted the simple, but grid

Table 1
Effect of numerical treatment of temperature discontinuity at corner points. Values between brackets indicate % difference with reference to the case of $\Delta L_{\text{lin}} = 0.025$ for CC configuration at $Ra = 5000$

Angle (Y)	Number of grid points	Nu-top surface	(%)	Nu-bottom surface	(%)	$v_{\max}$	(%)	$u_{\max}$	(%)	$\psi_{\max}$	(%)	Q_{error}
$\Delta L_{\text{lin}} = 0.075$												
0	62×282	1.97	(0.00)	2.80	(−10.83)	26.3	(0.00)	25.5	(0.00)	8.1	(0.00)	−0.03
30	62×282	1.63	(0.00)	2.40	(−12.73)	15.7	(0.00)	35.1	(0.00)	11.0	(0.00)	−0.04
60	62×282	1.37	(0.00)	2.37	(−12.87)	14.8	(0.00)	44.9	(0.22)	14.0	(0.00)	−0.03
90	62×282	1.24	(0.00)	2.39	(−12.45)	18.5	(0.00)	46.4	(0.00)	14.4	(0.00)	−0.02
$\Delta L_{\text{lin}} = 0.025$												
0	62×242	1.97		3.14		26.3		25.5		8.1		−0.17
30	62×242	1.63		2.75		15.7		35.1		11.0		−0.19
60	62×242	1.37		2.72		14.8		44.8		14.0		−0.19
90	62×242	1.24		2.73		18.5		46.4		14.4		−0.18
$\Delta L_{\text{lin}} = 0$												
0	62×282	1.97	(0.00)	4.00	(27.39)	26.3	(0.00)	25.5	(0.00)	8.1	(0.00)	−0.08
30	62×282	1.63	(0.00)	3.60	(30.91)	15.7	(0.00)	35.1	(0.00)	11.0	(0.00)	−0.09
60	62×282	1.37	(0.00)	3.57	(31.25)	14.8	(0.00)	44.9	(0.22)	14.0	(0.00)	−0.09
90	62×282	1.24	(0.00)	3.59	(31.50)	18.5	(0.00)	46.4	(0.00)	14.4	(0.00)	−0.08

Table 2
Results of grid dependence test for configuration CC at $Ra = 10^4$ and at inclination angles = 0, 30, 60, and 90 degree, $\Delta L_{\text{lin}} = 0.025$. Values between brackets indicate % difference with reference to the 62×242 grid

Angle (Y)	Number of grid points	Nu-top surface	(%)	$v_{\max}$	(%)	$u_{\max}$	(%)	Q_{error}
0	22×82	2.47	(0.00)	45.0	(−2.39)	40.9	(−3.99)	−0.49
30	22×82	2.09	(0.48)	27.1	(1.50)	56.3	(−1.23)	−0.56
60	22×82	1.79	(1.13)	22.1	(1.38)	69.5	(−1.84)	−0.50
90	22×82	1.55	(1.31)	26.8	(1.52)	72.5	(−1.49)	−0.39
0	42×162	2.46	(−0.40)	46.0	(−0.22)	42.3	(−0.70)	−0.24
30	42×162	2.08	(0.00)	26.8	(0.37)	57.1	(0.18)	−0.27
60	42×162	1.78	(0.56)	21.8	(0.00)	70.7	(−0.14)	−0.26
90	42×162	1.54	(0.65)	26.5	(0.38)	73.5	(−0.14)	−0.23
0	62×242	2.47		46.1		42.6		−0.15
30	62×242	2.08		26.7		57.0		−0.17
60	62×242	1.77		21.8		70.8		−0.17
90	62×242	1.53		26.4		73.6		−0.16
0	82×322	2.47	(0.00)	46.2	(0.22)	42.7	(0.23)	−0.11
30	82×322	2.08	(0.00)	26.7	(0.00)	57.2	(0.35)	−0.12
60	82×322	1.77	(0.00)	21.7	(−0.46)	70.8	(0.00)	−0.12
90	82×322	1.53	(0.00)	26.4	(0.00)	73.5	(−0.14)	−0.12

dependent, procedure by taking temperature at corner points as average temperature of the two intersecting walls and keeping temperatures of the adjacent nodal points at the respective wall temperatures. Following a procedure similar to that reported in [11], temperature of each corner point is taken as the average of the temperatures of the two intersecting walls. A linear temperature profile between the corner nodal point and a nodal point located at a small distance ΔL_{lin} along each wall is assumed. The value of ΔL_{lin} has been varied and its effect on the calculated flow and thermal fields has been examined. Table 1 presents the effect of ΔL_{lin} at 0, 0.025 and 0.075. Results reported in Table 1 and distributions of local Nusselt number shown in Fig. 4 confirm that the introduction of such linear temperature profile across ΔL_{lin} from the corner did not cause any significant changes in the calculated flow and internal thermal fields, and hence it did not affect flow-mode transition and hysteresis phenomena. However, the use of such linear profile made it possible to carry out grid dependence test and determine suitable size of the computational grid.

6. Grid dependence test

In thermal convection problems grid density strongly depend on Rayleigh number. For an inclined enclosure, grid density also depends on flow patterns, which in turns strongly depend on the cavity angle of inclination. A grid dependence test was performed for the cases of $Ra = 10^3$ and 10^4, considering all four configurations AA, CH, CC and HH. For each configura-

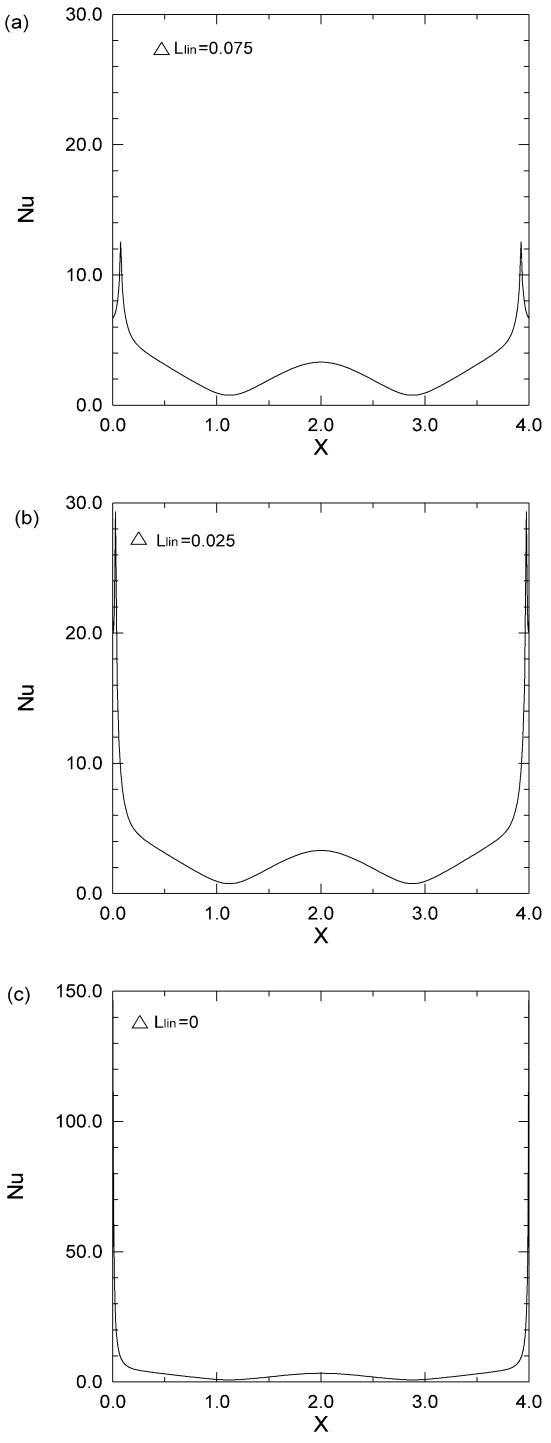

Fig. 4. Local Nusselt number at the bottom wall for (a) $\Delta L_{\text{lin}} = 0.075$; (b) $\Delta L_{\text{lin}} = 0.025$; (c) $\Delta L_{\text{lin}} = 0$ for CC configuration at $Ra = 5000$.

tion, grid test was performed at four angles of inclination, 0°, 30°, 60° and 90°. A sample of the results of this grid dependence test of the average Nusselt number at the cavity top wall, the maximum velocities $u_{\max}$ and $v_{\max}$, and the error in energy balance Q_{error} at $Ra = 10^4$ in the case of configuration CC is listed in Table 2. The 62×242 grid was found appropriate for all configurations considered in the present study. All results reported here have been obtained using a 62×242 grid and $\Delta L_{\text{lin}} = 0.025$.

7. Procedure of numerical calculations

Since mode transition is very sensitive to initial conditions or initial guess as indicated in [5,6] and the investigation of the hysteresis phenomenon is one of the major objectives of the present study, the sequence used to carry out the numerical calculations will be specified clearly. In calculations of the case of γ increasing from 0° to 90°, flow and temperature fields at a constant Ra and $\gamma = 0°$ are first calculated using 0 as initial guess for the velocity and the temperature fields. The $\gamma = 0°$ solution is then used as initial condition for solution of the subsequent case of inclination with $\gamma = 5°$, which is then used as an initial condition for the subsequent case of $\gamma = 10°$, and so on. As the value of γ at which mode-transition occurs is determined, say between 30° and 35°, calculations are then repeated starting from 30° with increments of 1° in order to locate mode-transition angle within 1° accuracy. A similar procedure is employed for calculations with γ decreasing starting from 90° back to 0°, using the 90° solution obtained from the γ increasing case as an initial condition for $\gamma = 85°$ and so on.

In order to check the accuracy of the results obtained using the present numerical algorithm, results were compared with those available in the literature. Numerical results of flow and thermal fields and average Nusselt numbers obtained for configuration AA at Rayleigh numbers between 2000 and 10^4, $A = 4$, $Pr = 0.7$, and γ between 0° to 90° were compared and found in good agreement with those reported by Soong et al. [8]. Although a good agreement between flow fields and internal temperature distributions calculated using the present numerical algorithm and those reported in [7] for $\gamma = 0°$ was found, Nusselt numbers reported in [7], did not agree with those obtained in the present study. This might be attributed to the difference in the way temperature discontinuities at corner points have been treated in the present study.

8. Results and discussion

All results reported here have been obtained for the case of cavity aspect ratio $A = 4$ and $Pr = 0.7$. Since streamlines and isothermal lines of configurations CC and HH are symmetric about the mid-plane of the horizontal wall, as reported in [7,12], and as evident by results shown here in Figs. 5, 6(a) and 6(e), for the sake of briefness, only results obtained for CC configuration will be presented here.

8.1. Effect of bidirectional temperature gradients on flow mode-transition during increasing of γ

With the bottom wall at a higher temperature than that of the top wall, two different modes of flow are expected; stationary longitudinal multi-cells with axes oriented up the slope driven by the cross temperature gradient; and a unicell-mode driven primarily by the upslope temperature gradient. Transition from one mode to the other depends on Rayleigh number, the angle of inclination; and expectedly on the configuration of bidirectional temperature gradients (i.e., on thermal conditions of the two end walls).

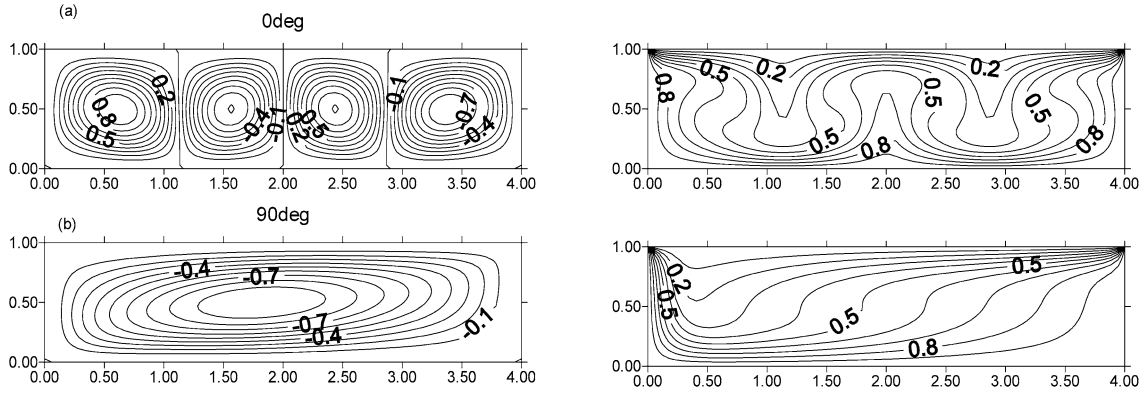

Fig. 5. Normalized streamlines and isothermal lines for HH case at $Ra = 10^4$. Positive values indicate rotation in clockwise direction. (a) $|\psi_{\max}| = 13.1$, (b) $|\psi_{\max}| = 22.3$.

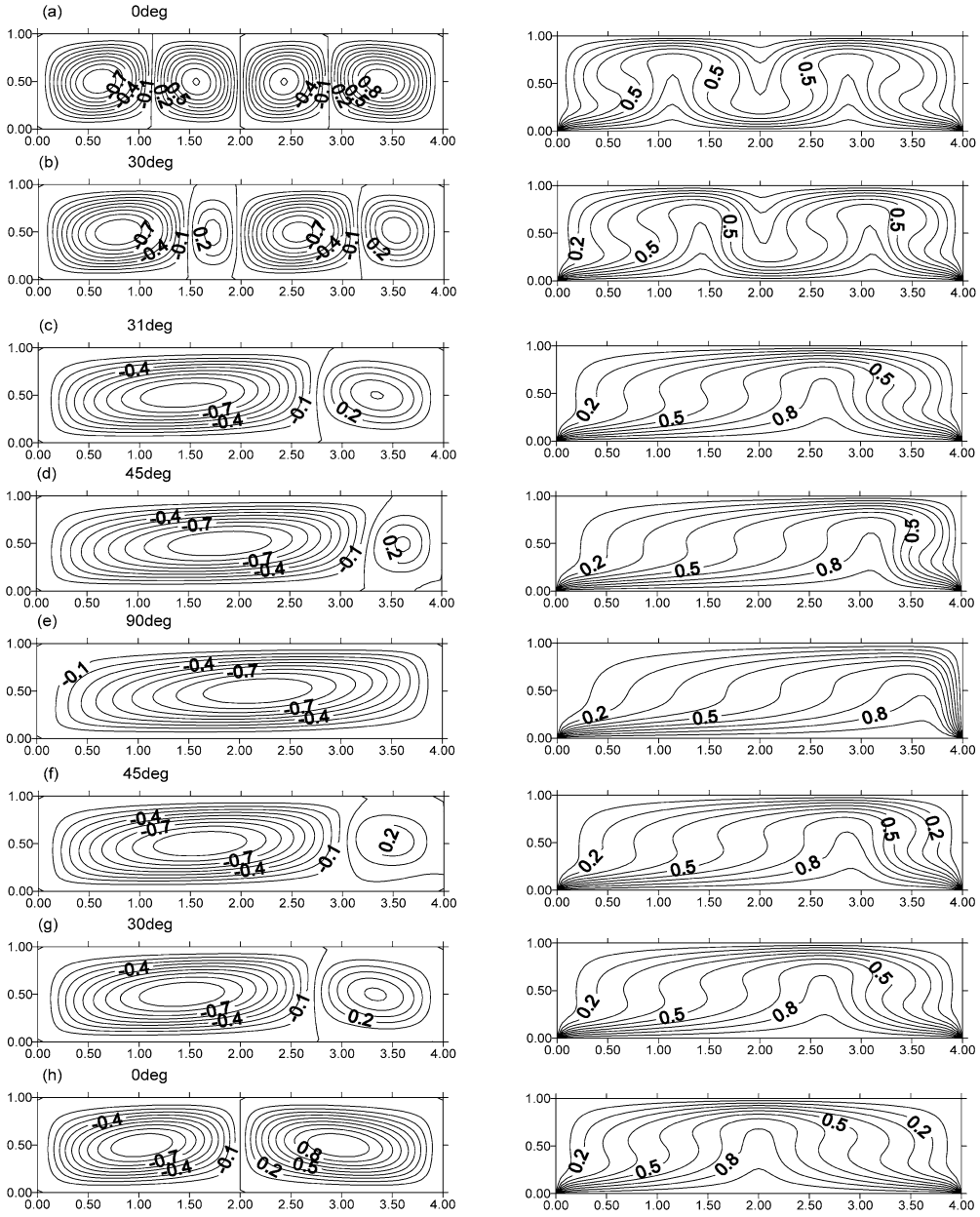

Fig. 6. Normalized streamlines and isothermal lines for CC case at $Ra = 10^4$. Positive values indicate rotation in clockwise direction. (a) $|\psi_{\max}| = 13.1$, (b) $|\psi_{\max}| = 15.0$, (c) $|\psi_{\max}| = 17.8$, (d) $|\psi_{\max}| = 19.4$, (e) $|\psi_{\max}| = 22.3$, (f) $|\psi_{\max}| = 19.3$, (g) $|\psi_{\max}| = 17.6$, (h) $|\psi_{\max}| = 13.5$.

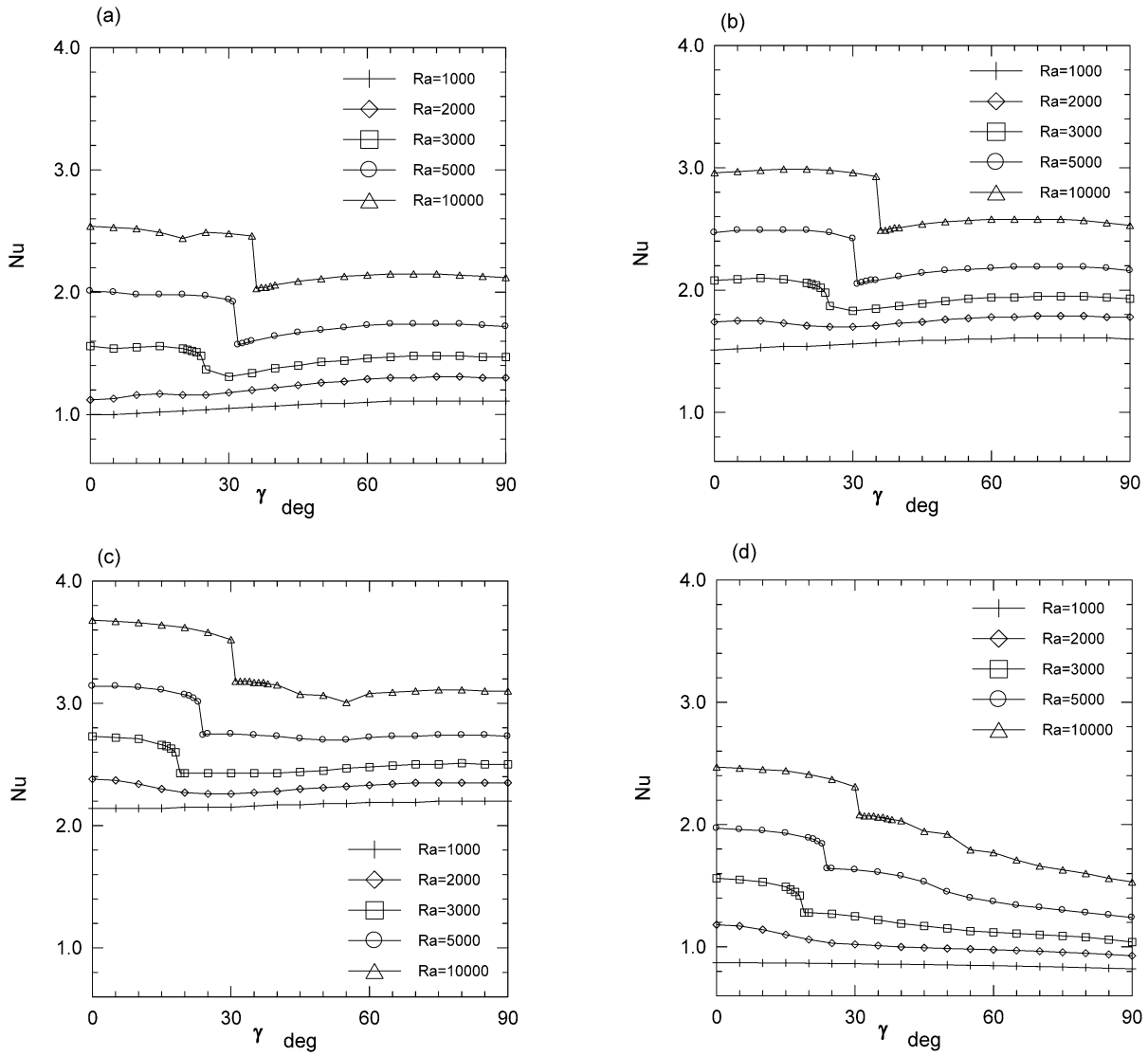

Fig. 7. Average Nusselt number at various inclination angles for AA, CH, CC (HH) Configurations, $A = 4$ and $Pr = 0.7$. (a) Nu on the top and the bottom walls for AA, (b) Nu on the top and the bottom walls for CH, (c) Nu at the bottom wall for CC (top wall for HH), (d) Nu on the top wall for CC (bottom wall for HH).

Only results obtained for the case of increasing γ will be discussed in this section. In which case, γ was increased starting from the cavity at the horizontal position (i.e., $\gamma = 0°$) all the way up to $\gamma = 90°$. Results of the case of decreasing γ from 90° back to 0° will be presented in Section 8.3 during the discussion of the hysteresis phenomenon.

AA configuration. Fig. 7(a) shows average Nusselt number at various Rayleigh numbers and inclination angles between 0° to 90° for AA configuration. At Rayleigh number below the critical value of about 1800, no convection was observed at $\gamma = 0°$; and conduction was the dominating mode of heat transfer, where *Nu* equals to one. For a higher Rayleigh number, convection contributed immediately as evident by the value of Nusselt number. As *Ra* further increased, a noticeable drop in Nusselt number appeared as γ was increased. This drastic change in the rate of heat transfer implied a mode-transition of the flow pattern. Fig. 7(a) also indicates that the angle at which mode transition took place depends on the value of Rayleigh number. As *Ra* increased, mode-transition was delayed, i.e., took place at a larger angle of inclination.

Fig. 8 presents the normalized streamlines and the isothermal lines for $Ra = 10^4$. At each angle of inclination, streamlines were normalized using the corresponding absolute maximum value of stream function, $|\psi_{\max}|$. At $\gamma = 0°$, a multi-cell flow pattern was observed. As γ increased slightly above 20°, the upslope temperature gradient caused a change in the number of cells from four to three, which resulted in a slight drop in Nusselt number as shown in Fig. 7(a). As γ increased further to 35°, the multi-cell flow structure was completely damped by the development of a stable upslope temperature gradient in the mean flow resulting into a unicell-flow pattern at $\gamma = 36°$, and therefore, into a drastic drop in Nusselt number as shown in Fig. 7(a). The unicell-mode prevailed all the way till the cavity assumed the vertical position (i.e., $\gamma = 90°$) where Nusselt number remained almost unchanged between $\gamma = 36°$ and 90°, Fig. 7(a).

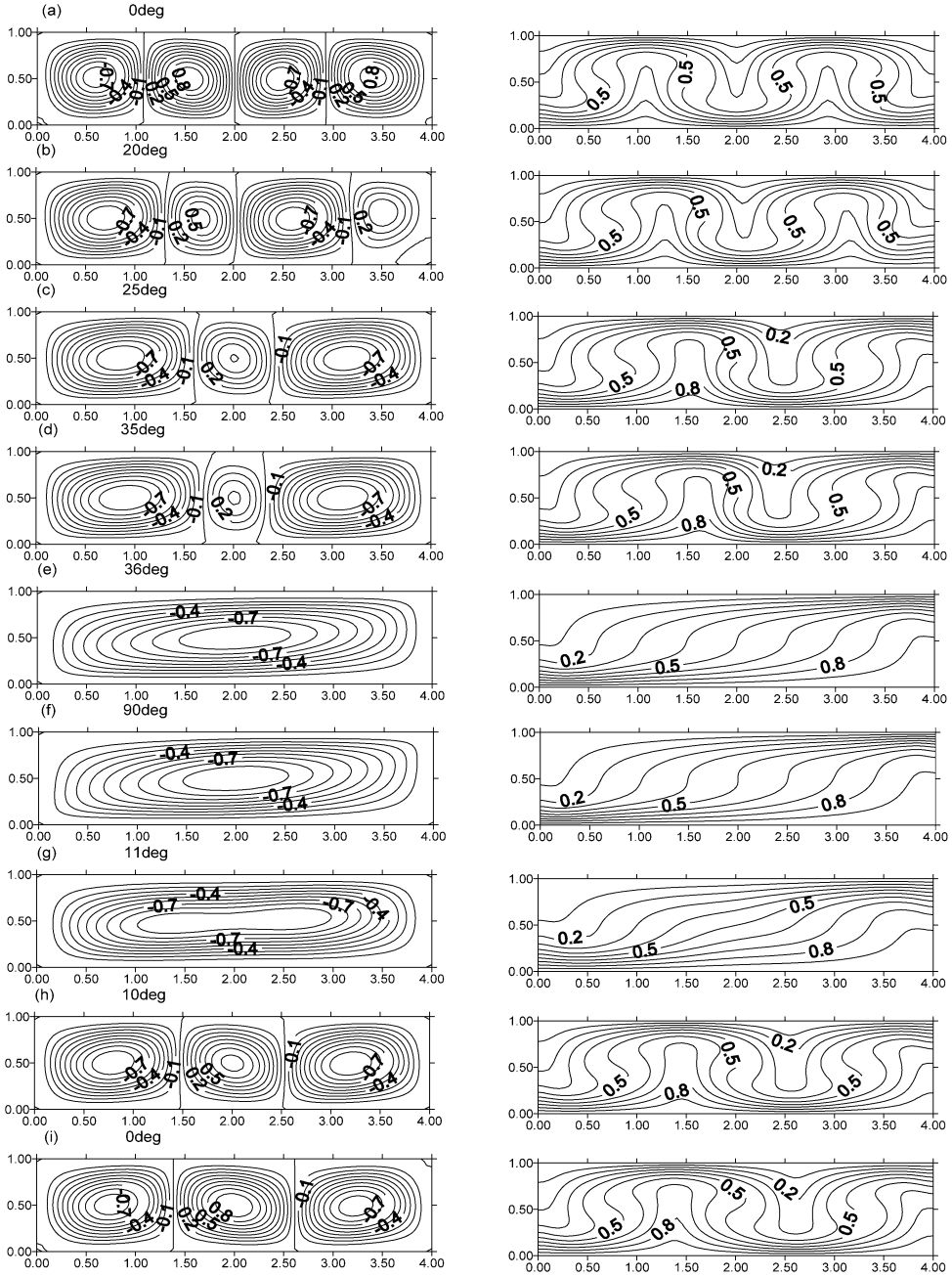

Fig. 8. Normalized streamlines and isothermal lines for AA case at $Ra = 10^4$. Positive values indicate rotation in clockwise direction. (a) $|\psi_{max}| = 12.3$, (b) $|\psi_{max}| = 14.3$, (c) $|\psi_{max}| = 15.5$, (d) $|\psi_{max}| = 15.9$, (e) $|\psi_{max}| = 19.8$, (f) $|\psi_{max}| = 21.4$, (g) $|\psi_{max}| = 12.6$, (h) $|\psi_{max}| = 14.4$, (i) $|\psi_{max}| = 13.5$.

CH configuration. Fig. 7(b) shows average Nusselt number at various Rayleigh numbers and inclination angles between 0° and 90° for CH configuration. Fig. 9 shows normalized streamlines and isothermal lines for $Ra = 10^4$. Due to the horizontal temperature gradients at the two end walls, convection contributes immediately even at *Ra* below the critical limit ($Ra = 1800$). These temperature gradients are also responsible for the development of a three-cell flow pattern that is much stronger than the one observed in Fig. 8, for the AA case, as evident from the noticeable increases in average Nusselt number and in the values of $|\psi_{max}|$. Higher flow velocities always produce fewer cells, and visa versa. No drop in Nusselt number is observed in this case around $\gamma = 20°$, as was for the AA case when the number of cells decreased from 4 to 3, see Figs. 7(a) and 8. Mode transition from multi-cell to unicell took place at $\gamma = 35°$, which is at the same value observed in the AA case.

CC and HH configurations. Figs. 7(c) and 7(d) present average Nusselt number *Vs* Rayleigh number at angles of inclination between 0° and 90° for CC and HH configurations. Fig. 6 shows streamlines and isothermal lines at $Re = 10^4$ for CC configuration. At $\gamma = 0°$, a four-cell flow pattern is observed. As the cavity is inclined, i.e., γ increased, temperature gradient at the right side wall produced a downward force that resulted into a clockwise rotating cell. At $\gamma = 30°$, transition in flow

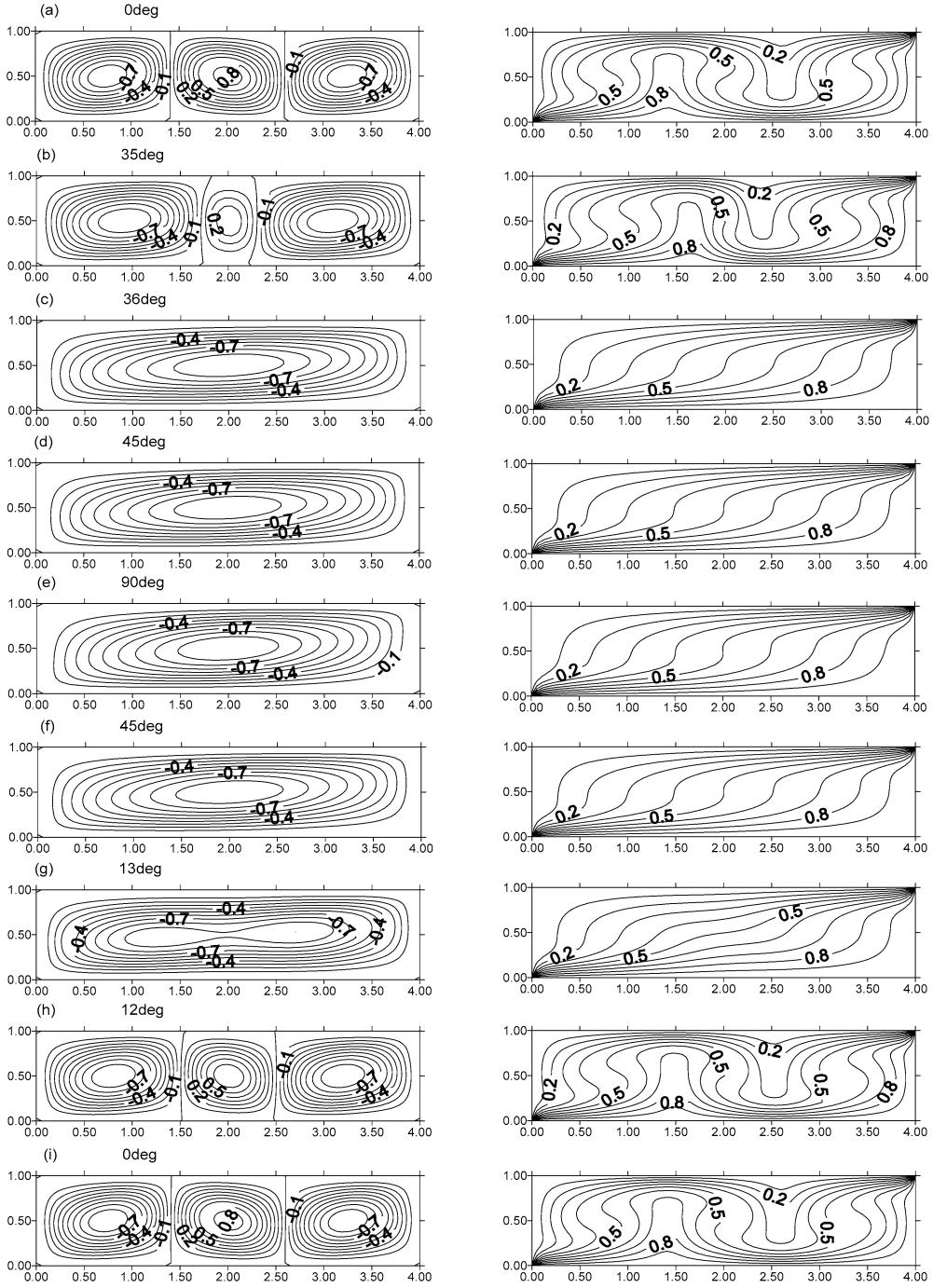

Fig. 9. Normalized streamlines and isothermal lines for CH case at $Ra = 10^4$. Positive values indicate rotation in clockwise direction. (a) $|\psi_{\max}| = 13.9$, (b) $|\psi_{\max}| = 15.9$, (c) $|\psi_{\max}| = 19.7$, (d) $|\psi_{\max}| = 20.8$, (e) $|\psi_{\max}| = 21.0$, (f) $|\psi_{\max}| = 20.8$, (g) $|\psi_{\max}| = 13.4$, (h) $|\psi_{\max}| = 14.8$, (i) $|\psi_{\max}| = 13.9$.

pattern took place, which reduced the number of cells to only two. This transition caused a sudden drop in average Nusselt number of the top and bottom walls, as shown in Figs. 6(c) and 6(d). The whole cavity was then occupied by one cell; except at the right corner, where the downward force caused by thermal condition of the right wall helped in sustaining that clockwise rotating cell. The two opposing forces, the one caused by the upward temperature gradient and the downward force caused by the cold right wall co-existed until $\gamma = 45°$, at which time that clockwise rotating cell could not resist the upward flow coming from the hot bottom wall and, then, was smeared out, at which time the whole cavity was occupied by a unicell-flow pattern.

8.2. Effect of bidirectional temperature gradients on heat transfer rates

With reference to the base case of unidirectional differential heating, AA configuration (Fig. 7(a)), as the two insulated end walls were replaced by cold and hot ones, as in CH configu-

ration, heat transfer effectiveness of both top and bottom walls increased by about 25% for Rayleigh numbers above the subcritical limit ($Ra > 1800$), refer to Figs. 7(a) and 7(b). For lower Rayleigh numbers ($Ra < 1800$), heat transfer effectiveness increased by about 50% due to convective contribution caused by temperature gradients at the two end walls.

As both insulated end walls were replaced by cold walls, configuration CC, heat transfer effectiveness of the bottom wall increased by about 50% for Rayleigh numbers above the subcritical limit, refer to Figs. 7(a) and 7(c), and by more than 100% for lower Rayleigh numbers. However, at $\gamma = 0°$, heat transfer effectiveness of the top wall for *Ra* numbers 3000 and above slightly decreased. For $Ra = 2000$, it increased by about 10%, while decreased by about 40% at $Ra = 1000$. These results warrant a closer look at the effect of the two cold walls on flow patterns, and hence on effectiveness of heat transfer of the top wall.

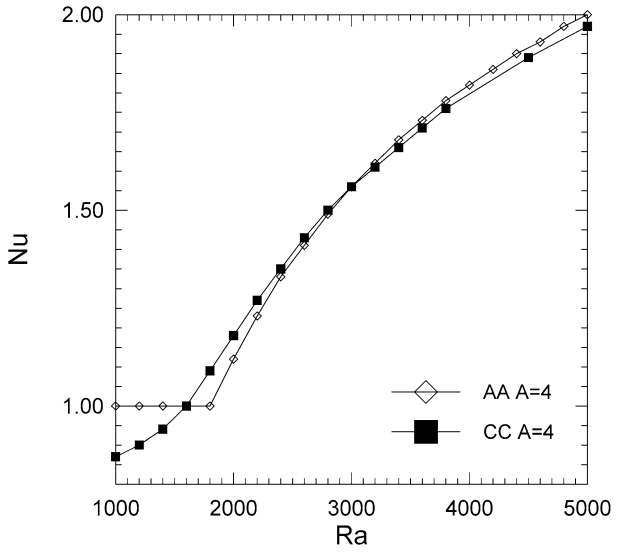

Fig. 10. Average Nusselt number of the top wall Vs Rayleigh number at $\gamma = 0°$ (horizontal position), $A = 4$, and $Pr = 0.7$ for AA and CC configurations.

Fig. 10 shows average Nusselt number of top wall at $\gamma = 0°$ for *Ra* between 1000 and 5000. At *Ra* below the critical value, the two cold walls promoted convection at the two ends of the cavity. At the middle of the cavity, heat transfer was still dominated by conduction, which caused a decrease in the amount of heat transfer from the top wall. At $Ra = 1600$, convection flow produced by the two cold walls strengthened the cross temperature gradient producing a multi-cell flow at the middle of the cavity, which enhanced effectiveness of heat transfer from top wall. This effect has been observed until $Ra = 3000$, at which time the cross temperature gradient and the resulted multi-cell flow has become strong enough for heat to be transferred from the bottom wall to the top wall. As Ra increased further, the pre-cooling caused by the two cold side walls resulted into a slight decrease in the effectiveness of heat transfer of the top wall.

Figs. 11 and 12 show a comparison between vertical velocity distribution, V, at $y = H/2$ and local Nusselt number of the top wall at $Ra = 1000$, 2000, and 5000, and $\gamma = 0°$ for AA and CC configurations. In case of CC configuration, a noticeable increase in the vertical velocity can be observed when *Ra* increased from 1000 to 2000, as compared with AA configuration. As *Ra* further increased from 2000 to 5000, values of V have not noticeably changed.

In the case of CC configuration, increasing the angle of inclination, γ, resulted into an early mode-transition from multi-cell to unicell, where the pre-cooling effect of the two cold walls lead to a significant decrease in heat transfer effectiveness of top wall. That decrease reached its maximum limit when the cavity reached its vertical position, i.e. at $\gamma = 90°$, as shown in Figs. 7(a) and 7(d).

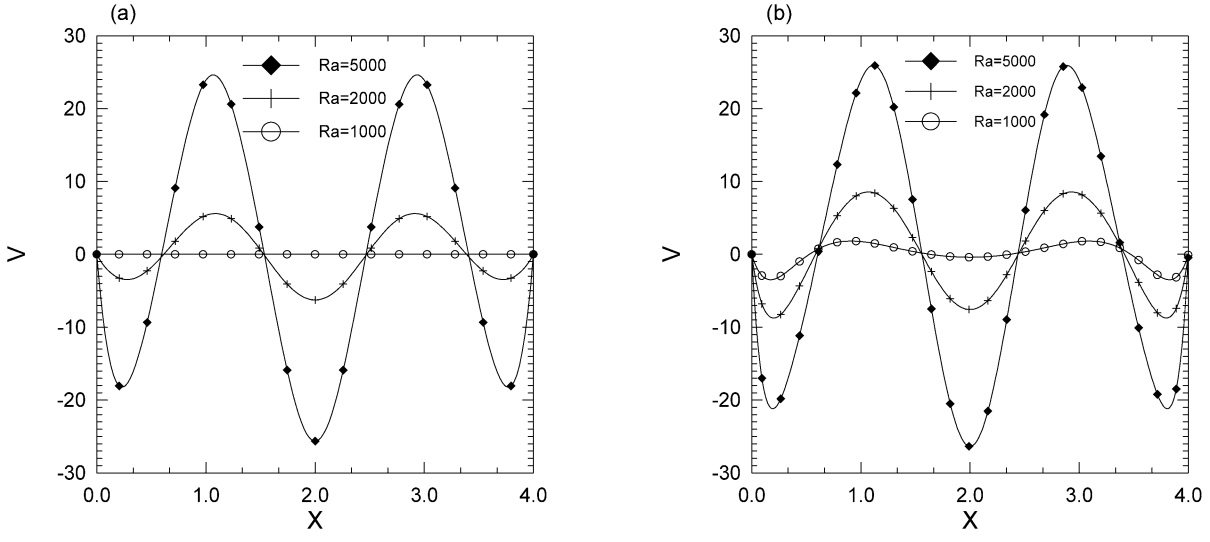

Fig. 11. Vertical velocity distribution for AA and CC configurations at $y = 0.5$, $\gamma = 0°$ (horizontal position), $A = 4$, $Pr = 0.7$, and $Ra = 1000$, 2000, 5000, (a) AA configuration, (b) CC configuration.

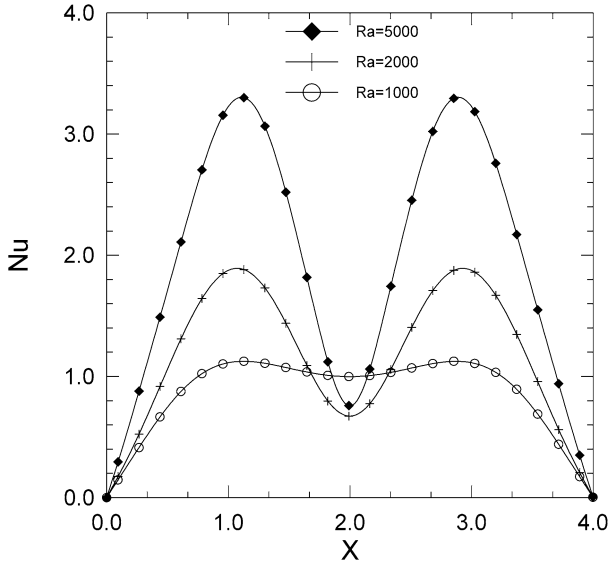

Fig. 12. Distribution of local Nusselt number of the top wall in the case of CC configuration, $\gamma = 0°$ (horizontal position), $A = 4$, $Pr = 0.7$, and $Ra = 1000$, 2000, and 5000.

8.3. Effect of bidirectional temperature gradients on hysteresis phenomenon

As shown in Section 8.1, flow patterns in inclined cavities, heated from bottom, cooled from top; with insulated end walls, can be characterized as highly nonlinear flows, where dual or multiple solutions may exist. These multiple solutions might also change character depending on the direction of change of angle of inclination, increasing or decreasing, which is defined as a hysteresis phenomenon. For the case of insulated end walls, this phenomenon has been observed in some ranges of angle of inclination as reported in [8]. It has mainly been attributed to the effect of initial conditions of fluid inside the cavity.

In the present study, in order to investigate the effect of various bidirectional temperature gradients on such hysteresis phenomenon, computations started with the cavity in the horizontal position, i.e., $\gamma = 0°$ and γ was increased by 5° until $\gamma = 90°$. Using the solution at $\gamma = 90°$ as initial condition, the sequence of computations was then reversed, i.e., γ was decreased, again in steps of 5°, until the cavity was brought back to the horizontal position. In each case of γ increasing and de-

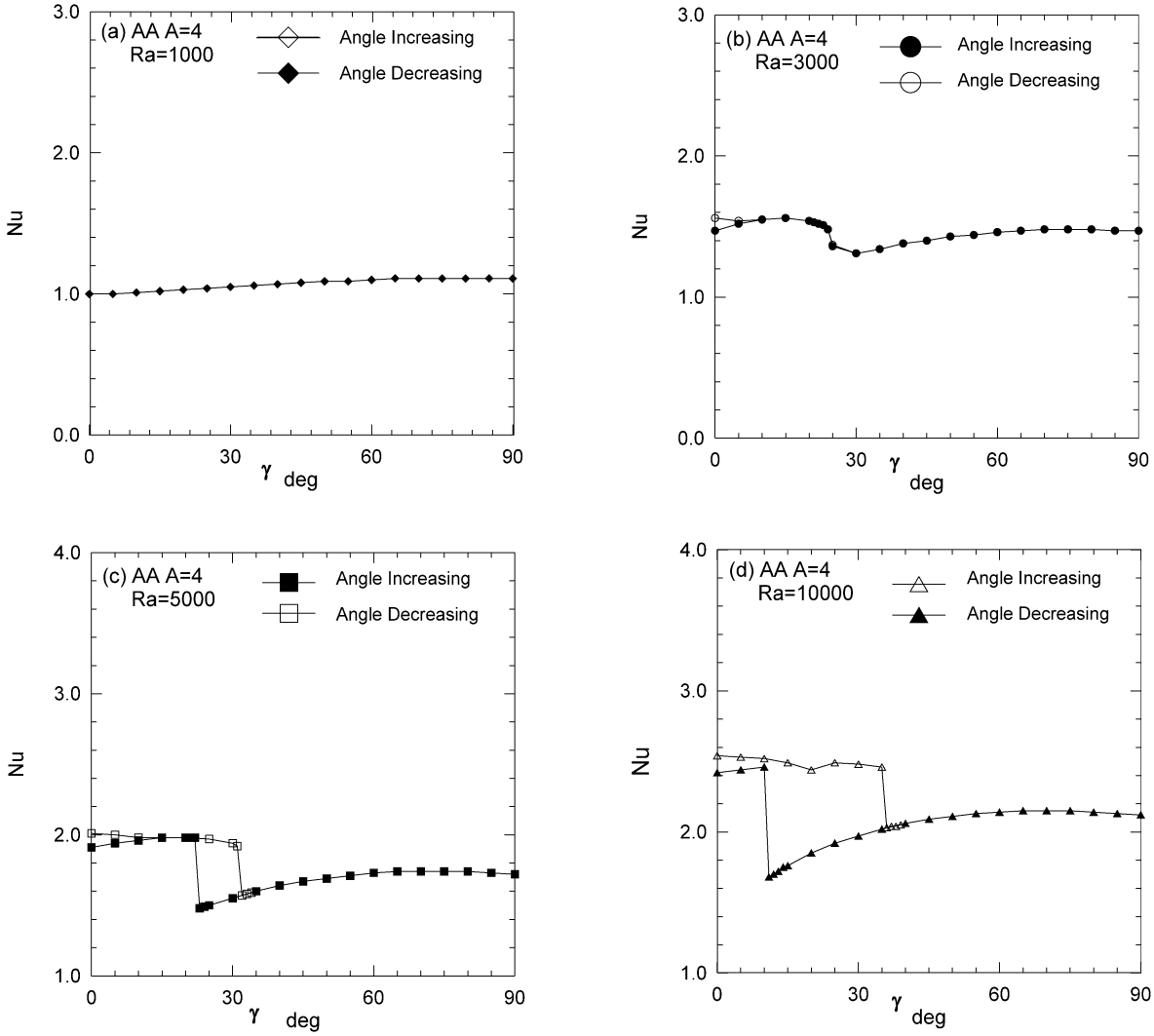

Fig. 13. Average Nusselt number for the case of angle increasing and decreasing for AA configuration at various Rayleigh numbers, $A = 4$, and $Pr = 0.7$.

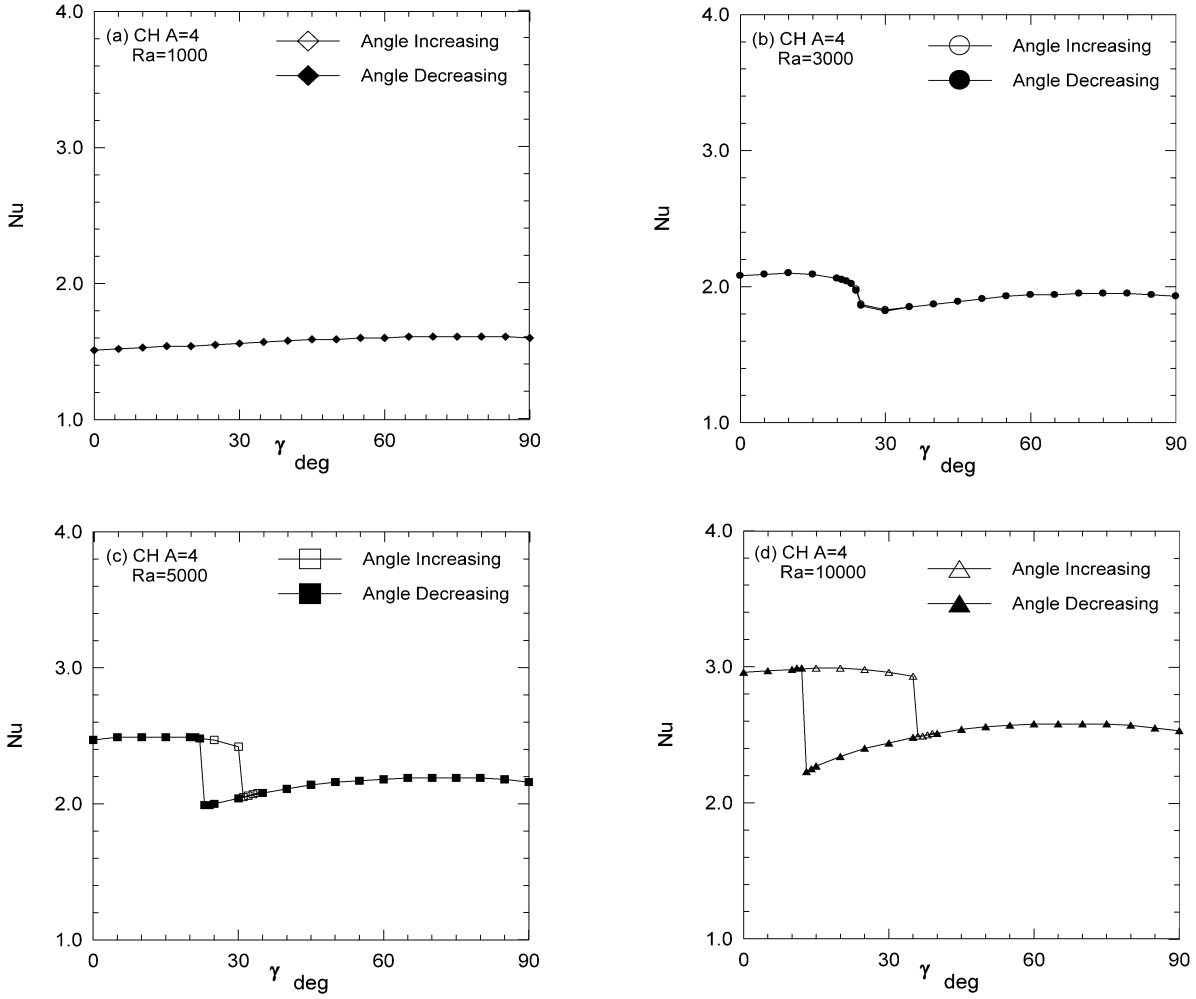

Fig. 14. Average Nusselt number for the case of angle increasing and decreasing for CH configuration at various Rayleigh numbers, $A = 4$, and $Pr = 0.7$.

creasing, as the value of γ at which mode-transition occurs was determined, say between 30° and 35°, calculations were then repeated starting from 30°, or from 35° in case of decreasing γ, with increments of 1° in order to locate mode-transition angle within 1° accuracy.

Results of computations carried out for the four configurations of bidirectional temperature gradients considered in the present study are discussed below.

AA configuration. Fig. 13 shows calculated average Nusselt number for the two cases of increasing and decreasing γ. At $Ra = 1000$, Fig. 13(a), no significant difference between results obtained in the two courses of changing γ was observed. At $Ra = 3000$, Fig. 13(b), two solutions deviate in a small region of inclination around $\gamma < 10°$. For $Ra = 5000$, the first hysteresis region extends to higher angles, $\gamma < 15°$, and another hysteresis region appears around $\gamma = 30°$, Fig. 13(c). At $Ra = 10^4$, the two dual solution regions enlarge and merge together as shown in Fig. 13(d).

Referring back to Fig. 8, in the case of increasing γ, four cells were observed at $\gamma = 0°$, see Fig. 8(a). During the course of increasing γ, mode transition took place twice, from four to three cells at $\gamma = 20°$ (Fig. 8(b)), and at $\gamma = 35°$ (Fig. 8(d)) at which case a three-cell flow pattern merged into a unicell flow pattern. However, during the course of decreasing γ, mode transition occurred only once at $\gamma = 10°$, where a unicell flow pattern split into a three-cell flow structure, as shown in Fig. 8(h).

This difference observed in the values of the angle of inclination at which mode transition took place; and in the resulted flow patterns for the two case of increasing and decreasing γ, are attributed to the difference in the initial conditions at which mode transition took place, and hence, on the resulted flow and thermal fields.

In the case of increasing γ, the solution at $\gamma = 0°$ was obtained by assuming zero initial flow velocity and initial temperature $= T_c$ (i.e., $\theta = 0$), everywhere. The absolute maximum value of the steam function, $|\psi|_{\max}$, of the resulted four-cell flow field was 12.3, Fig. 8(a). At $\gamma = 10°$, $|\psi|_{\max}$ was 13.3. Transition to unicell took place at $\gamma = 35°$, where $|\psi|_{\max} = 15.9$. In the case of decreasing γ, at $\gamma = 35°$, the resulted flow field had higher flow velocities as evident from the value of $|\psi|_{\max} = 19.6$, which is about 40% higher than that obtained in the case of increasing γ. This high-velocity flow field was able to occupy the whole cavity, and therefore, resulted in a unicell flow pattern. This is the reason why mode transition to multicell, in the case of decreasing γ, was delayed until γ reached

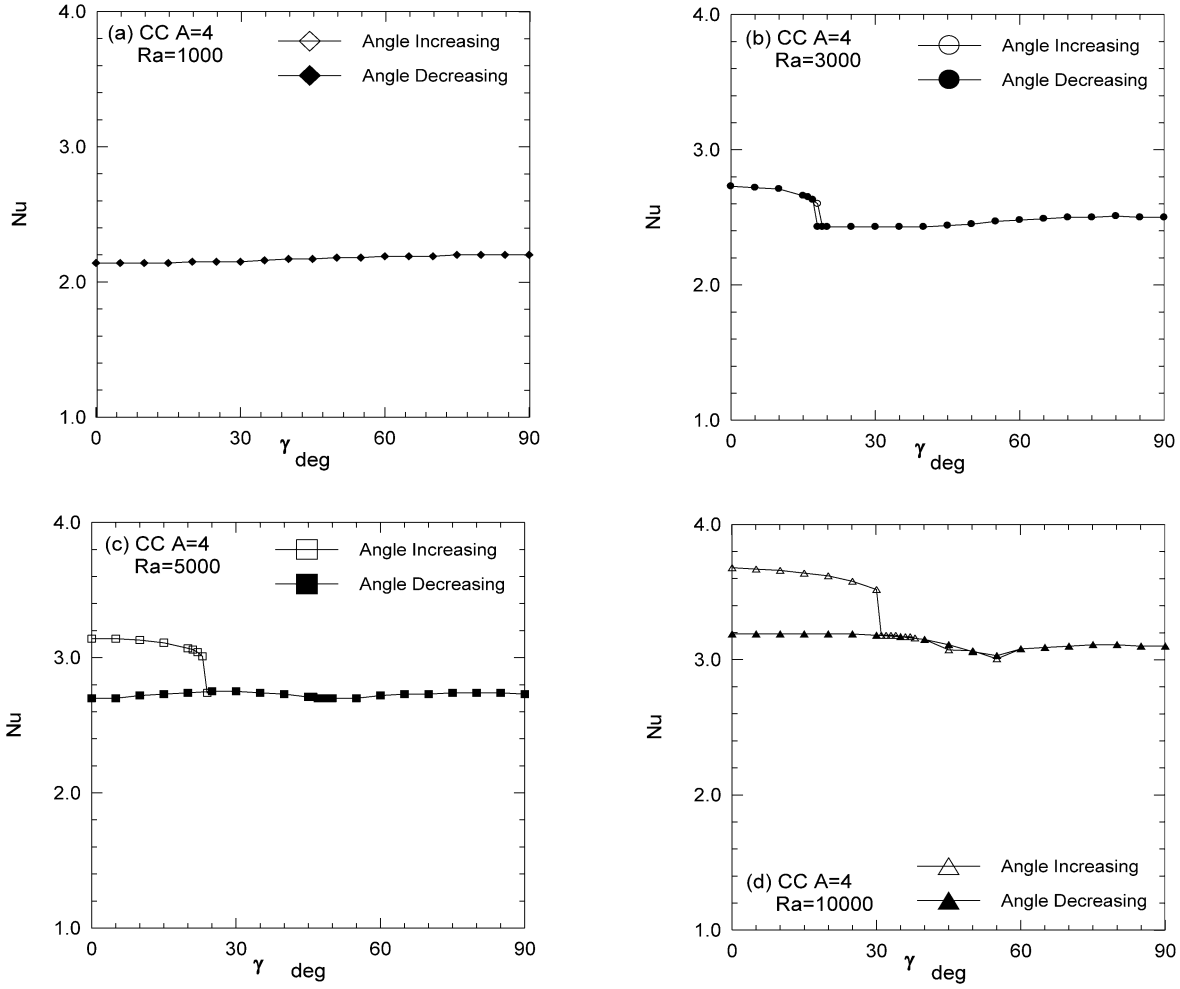

Fig. 15. Average Nusselt number for the case of angle increasing and decreasing for CC configuration at various Rayleigh numbers, $A = 4$, and $Pr = 0.7$.

a value between 11° and 10°. Even after mode transition took place, the resulted flow fields were characterized by higher flow velocities, as evident from the values of $|\psi|_{\max} = 14.4$ and 13.5 obtained at $\gamma = 10°$ and 0°, respectively.

CH configuration. Fig. 14 shows calculated average Nusselt number for the two cases of increasing and decreasing γ for CH configuration. At $Ra \leqslant 3000$, no significant difference between the results obtained in the two courses of changing γ was observed as shown in Figs. 14(a) and 14(b). At $Ra = 5000$, Fig. 14(c), two solutions deviate in a small region of inclination around γ between 20° and 30°. For $Ra = 10^4$, the range of γ, at which hysteresis region exists, extends to higher angles between 10° and 35°, as shown in Fig. 14(d).

As illustrated in Fig. 9(a) for the case of increasing γ, at $\gamma = 0°$, thermal conditions of the two end walls resulted in higher flow velocities, as evident from the value of $|\psi|_{\max} = 13.9$, which is about 13% higher than that obtained for AA configuration. As indicated before, flow fields with higher velocities always result in fewer cells, see Figs. 8(a) and 9(a). Mode transition took place at $\gamma = 35°$ where $|\psi|_{\max} = 15.9$.

In the case of decreasing γ, a unicell flow pattern dominated until $\gamma = 13°$. Here, it is worth noting that $|\psi|_{\max}$ at $\gamma = 35°$ was about 19.6, which is about 40% higher than that obtained in the case of increasing γ, and is almost equal to the value obtained in the case of AA configuration. Mode transition took place at $\gamma = 13°$ earlier than observed that in the case of AA configuration where it took place at $\gamma = 10°$. This early mode transition is attributed to the effect of temperature gradients at the end walls. These temperature gradients resulted in an increase in buoyancy force in the cross-stream direction (y-direction). The value of this force became high enough to overcome the effect of the other buoyancy force in the upslope direction (x-direction). This effect caused an early break-up of the unicell flow pattern, sustained by the upslope force, into a multi-cell structure, which is, on the other hand, sustained by the cross-stream buoyancy force.

CC and HH configurations. As mentioned before, since streamlines and isothermal lines of configurations CC and HH are symmetric about the mid-plane of the cavity, for the sake of briefness, only results obtained for CC configuration will be discussed below.

Fig. 15 presents calculated average Nusselt number for the two cases of increasing and decreasing γ for CC configuration. At $Ra \leqslant 3000$, no significant difference between the results ob-

tained in the two courses of changing γ was observed as shown in Figs. 15(a) and 15(b). At $Ra = 5000$, Fig. 15(c), two solutions deviate in a hysteresis region extending between $\gamma = 0°$ and about 25°. For $Ra = 10^4$, a hysteresis region similar to that observed for $Ra = 5000$ extends between $\gamma = 0°$ and about 30°. A second region of two solutions exists in the range of γ around 40° and 60 °, Fig. 15(d).

Referring back to Fig. 6(a), for the case of increasing γ, at $\gamma = 0°$ the two cold side walls resulted in relatively lower flow velocities than in the case of CH configuration, as evident from the value of $|\psi|_{\max} = 13.1$. This value is about 6% lower than that obtained in the case of CH configuration. As indicated before, flow fields with lower velocities always result in more cells and visa versa, see Figs. 9(a) and 6(a). Therefore, a four-cell flow pattern was obtained in the case of CC configuration. Mode transition to unicell was significantly delayed until $\gamma > 45°$, as shown in Fig. 6(d). This is believed to be due to the effect of temperature gradient at the right end wall. As the angle of inclination increased, component of buoyancy force in the cross-stream direction decreased. On the other hand, the other component in the upslope direction increased. As indicated before, the one in the cross-stream direction is responsible for the existence of multi-cell flow modes. Unicell flow modes are promoted and sustained by the existence of strong upslope components. The rate at which these two components exchange strength, as the angle of inclination changes, is the main parameter upon which mode transition strongly depends. Temperature gradients at the two end walls in the case of CC configuration resulted in a lower upslope component, which caused that significant delay in mode transition to unicell flow.

Upon decreasing γ, the effect of initial conditions on the resulted flow velocities was significant. At $\gamma = 30°$, $|\psi|_{\max}$ was 17.6, which is about 17% higher than its value of 15.0 obtained at the same angle of inclination during the case of increasing γ. As γ was decreased back to 0°, a two-cell flow pattern was observed, see Figs. 6(a) and 6(h). Flow fields with higher velocities result in fewer cells. This rule seemed to hold in this case as well.

9. Summary and conclusion

Steady, two-dimensional, natural convection in an air-filled rectangular enclosure has been numerically investigated using the finite-volume based SIMPLE numerical algorithm.

In addition to the base case of insulated end walls, three alternative configurations of bidirectional temperature gradients have been considered.

Numerical treatment of temperature discontinuities at the cavity corner points did not affect the predicted flow and internal thermal fields.

Bidirectional temperature gradients and the corresponding thermal conditions of the cavity two end walls have a significant effect on flow-mode transition of thermal convection flows; and on hysteresis phenomenon as the angle of inclination varied. Results showed that it is quite possible to alter the resulted heat transfer rates by adjusting these thermal conditions; by varying cavity angle of inclination, or by modifying initial conditions of fluid inside the cavity. These parameters offer important tools that one could use to control, device, or achieve certain heat transfer rates that might be required in many industrial applications where thermally driven flows inside inclined cavities play dominating roles.

Acknowledgements

The authors would like to acknowledge financial support of this work provided by the NSERC of Canada.

References

[1] G. De Vahl Davis, Natural convection in a square cavity: a comparison exercise, Int. J. Numer. Methods Fluids 3 (1983) 227–248.

[2] J.N. Arnold, I. Catton, D.K. Edwards, Experimental investigation of natural convection in inclined rectangular regions of differing aspect ratios, ASME J. Heat Transfer 98 (1976) 67–71.

[3] M.S. Elsherbiny, Free convection in inclined air layers, heated from above, Int. J. Heat Mass Transfer 39 (18) (1996) 3925–3930.

[4] S. Ostrach, Natural convection in enclosure, J. Heat Transfer Trans. ASME 110 (1988) 1175–1190.

[5] E.J. Hart, Stability of the flow in a differentially heated inclined box, J. Fluid Mech. 47 (3) (1971) 547–576.

[6] D. Mukutmoni, K.T. Yang, Flow transitions and pattern selection of the Rayleigh–Benard problem in rectangular enclosures, Sadhana – Academy Proceedings in Engineering Sciences 19 (5) (1994) 649–670.

[7] M. Corcione, Effects of the thermal boundary conditions at the sidewalls upon natural convection in rectangular enclosures heated from below and cooled from above, Int. J. Thermal Sci. 42 (2003) 199–208.

[8] C.Y. Song, P.Y. Tzeng, Numerical study on mode-transition of natural convection in differentially heated inclined enclosures, Int. J. Heat Mass Transfer 39 (14) (1996) 2869–2882.

[9] S.V. Patankar, Numerical Heat Transfer and Fluid Flow, McGraw-Hill, New York, 1980.

[10] M. Nansteel, S. Sadhal, P. Ayyaswamy, Discontinuous boundary temperatures in heat transfer theory, in: Session on Significant Questions in Buoyancy Affected Enclosure or Cavity Flows, ASME Winter Annual Meeting, December 1986.

[11] M.M. Ganzarolli, L.F. Milanez, Natural convection in rectangular enclosures heated from below and symmetrically cooled from the sides, Int. J. Heat Mass Transfer 38 (6) (1995) 1063–1073.

[12] M. Yang, W.Q. Tao, Q.W. Wang, S.S. Lui, On identical problems of natural convection in enclosures and applications of the identity character, J. Thermal Sci. 2 (2) (1993) 116–125.